The National Academies of
SCIENCES · ENGINEERING · MEDICINE

Developing a Long-Term Strategy for Low-Dose Radiation Research in the United States

PUBLIC MEETING #5 (Virtual)

The Future of Low-Dose Radiation Dosimetry: New Technologies

Wesley E. Bolch, PhD
University of Florida

UF | UNIVERSITY of FLORIDA
J. Crayton Pruitt Family Department of Biomedical Engineering

Methods of Dose Calculation (emphasis on internal emitters)

Unlike external radiation exposures – where the absorbed dose can often be measured (or inferred from measurements) – tissue absorbed dose must be calculated for internal exposures.

There are three principal approaches to computing tissue absorbed dose for internalized radionuclides

- ***Direct Monte Carlo (MC) radiation transport simulation***
- ***Dose point kernel (DPK) convolution***
- ***MIRD S-value formalism***

These methods should not be viewed as independent. For example, S values data must be determined by either MC or DPK convolution, whereas the DPK itself should be calculated either analytically or by direct MC. The DPK and MC approaches are also extensively used external medical irradiations (e.g, EBRT for cancer), whereas the S-value formalism is specific to internalized radionuclide / radiopharmaceutical exposures.

Methods of Dose Calculation

Direct MC is used extensively at the subcellular level (~nm to μm scale) – a setting in which the other two methods are not recommended. Owing to its high degree of accuracy, MC simulations are generally considered to be the "reference standard" for tissue dosimetry, and are the most reliable tool for computing radionuclide S-values.

DPK convolution is commonly used for dosimetry at the voxel level (~mm scale) which lies between the application regimes of the S-value (~cm) and direct MC (~nm to μm) methods. Because of its moderate computational effort (compared to MC), it is a method of choice for 3D absorbed dose calculation within organs and tumors deduced from emission tomography imaging (SPECT and PET). DPK convolution has emerged as the preferred tool for personalized dosimetry in the clinical setting. However, DPK-based voxel dosimetry is often implemented clinically via voxel S-values (which themselves are computed by DPK convolution).

S-values are the most practical of the three methods owing to its link to the MIRD schema. Although, in principle, it is applicable at any spatial scale, the underlying approximations of the method (standardized anatomy and uniform source/target regions) limit its use mostly to organs and suborgan levels (~cm scale).

1. Monte Carlo Radiation Transport Simulation

Main Advantages of the MC approach to tissue dosimetry is that it is directly applicable to:

- ***Inhomogeneous media (soft tissue – lung and soft tissue – bone interfaces)***
- ***Complex anatomic geometries (sub-regions of the brain for example)***
- ***Conditions where radiation (or charge-particle) equilibrium is not fulfilled (e.g., near these interfaces)***

Thus, MC simulations allow 3D absorbed-dose calculations for almost any volume within the patient's body.

An attractive feature of the MC method lies in its applicability to the entire range of targets of interest – from cm scale of human organs to mm scale of imaging voxels to μm and nm scale of cells and cell compartments.

Moreover, MC simulations have the potential to link different stages of radiation action (physics, chemistry, biology) ultimately contributing to the development of mechanistic bioeffect models of radiation action.

1. Monte Carlo Radiation Transport Simulation

Limitations of the MC approach include:

*(1) **Statistical limitations.** Only a finite number of histories can be simulated as CPU time increases. Solutions include moving from CPU to GPU computations, variance reduction techniques, and physics approximations to speed computation.*
*(2) **Low-energy cut-offs** must be set for particle transport to maintain reasonable CPU times.*
*(3) **Neglect of quantum mechanical uncertainties** regarding the "location" of interaction events.*

Two Methodologies for MC Radiation Transport

(1) Discrete Interaction Approach

In this approach, all interactions in the particle track are simulated as discrete events in a chronological order. The particle propagates in steps that represent the distance between successive interactions and the outcome of each step (e.g. scatting angle and/or energy loss) is determined by a particular single-scatting model.

(2) Condensed History Approach

In this approach, the particle track is divided into steps sufficiently long compared to the mean free path (MFP) for charged particle elastic scattering events, so that numerous interactions occur along each simulation step. Inelastic collisions are also "condensed" and are treated by concepts such as stopping power and straggling distributions.

1. Monte Carlo Radiation Transport Simulation

Common MC radiation transport codes:

ETRAN *(Berger 1963; 1988; Seltzer 1988)* ***–*** *code developed in 1963 as the first electron transport code to use condensed-history simulations. It is the electron transport engine within the widely used MCNP code (Briesmiester 1986).*

OEDIPE *(Chiavassa et al. 2005)* ***and SCMS*** *(Yoriyaz et al. 2001)* ***–*** *treatment planning software codes for personalized 3D dosimetry in RPT based upon MCNPX and MCNP4B respectively for absorbed dose calculation.*

Other widely used condensed-history codes:

GEANT4 *(Allison et al. 2016)****, EGSnrc*** *(EGSnrc 2020),* ***PENELOPE*** *(Baró et al. 1995)****, FLUKA*** *(Ferrari et al. 2005)****, PHITS*** *(Sato et al. 2018)*

EGS4 – *used in DOSE3D (Clairand et al. 1999) and 3D-RD (Song et al. 2007) TPS for personalized 3D dosimetry in RPT*

GEANT4 – *underlying MC engine of the GATE (Sarrut et al. 2014) simulation platform used in diagnostic and therapeutic NM*

GEANT4 – *underlying MC engine of the TOPAS (Perl et al. 2012) simulation platform used in charged-particle therapies*

Advanced track-structure codes:

NOREC – *ORNL and NIST (Semenenko et al. 2003)*

PARTRAC *– GSF / HMGU (Friedland et al. 2011)*

KURBUC *– Karolinska Institute (Nikjoo et al. 2016)*

2. Dose-Point Kernel Convolution

The dose-point kernel (or DPK) is commonly defined as the distribution of absorbed dose around an isotropic point source in an infinite homogeneous medium. The DPK is defined for any type of radiation (e.g., both charged and uncharged particles) and medium (e.g., water, air, soft tissue, and bone).

Assuming that the source is a point at r = 0, the defining relation is:

$$\boldsymbol{K(r) = \frac{\delta E(r)}{\delta m(r)}}$$

where $K(r)$ is the DPK (units of absorbed dose per emitted particle) at distance r, and $\delta E(r)$ is the energy absorbed in a spherical shell of radius r, mass $\delta m(r)$, and thickness δr.

The DPK may be directly linked to the MIRD formalism via the relation:

$$\boldsymbol{K(r) = E_0 \Phi(r)}$$

where E_0 is the energy of the particle emitted by the source and $\Phi(r)$ is the point isotopic specific absorbed fraction (in units of reciprocal mass).

2. Dose-Point Kernel Convolution

Because of the significantly different penetration ranges, it is common to distinguish between photon DPKs, electron DPKs, and alpha DPKs. In practice, photon DPKs are used for organ-level dosimetry (~cm scales) in which case both beta and alpha particles are considered as non-penetrating. Electron DPKs are the main input to voxel-level dosimetry (~mm scales) while alpha DPKs are used for subcellular, cellular, and multi-cellular level dosimetry.

Photon DPKs

The analytic expressions for the primary photon DPK and the total photon DPK are:

$$K_{pr}(r) = \frac{E_0}{4\pi r^2}\frac{\mu_{\mathrm{en}}}{\rho}e^{-\mu r}$$

$$K(r) = K_{pr}(r)B_{\mathrm{en}}(\mu r)$$

where μ and μ_{en} are the linear attenuation and energy absorption coefficients, respectively, of the photons in the material and B_{en} is the energy-absorption buildup factor that takes into account the contribution of scattered photons and depends upon the photon energy, the material (via μ), and the distance r from the source.

Charged Particle DPKs

The DPKs for monoenergetic charged-particles are calculated using the following:

$$K(r) = \frac{1}{4\pi r^2 \rho}\left.\frac{dE}{dX}\right|_{X(E_0)-r}$$

where dE/dX is the energy-loss per distance evaluated at $X(E_0) - r$ (i.e., at the residual range of the particle with initial kinetic energy E_0 after traveling distance r). The two quantities, dE/dX and $S = dE/dl$, are not the same because dX denotes a radial distance (i.e., along r) whereas dl represents a distance along the particle trajectory.

3. Radionuclide S-Values and the MIRD Schema

A third method of absorbed-dose calculation is the use of the S-value as defined within the framework of the MIRD schema. The S-value represents the mean absorbed dose to a defined target region r_T *per nuclear transformation of a radionuclide localized uniformly within a defined source region* r_S.

It is computed with required parameters being the energies and yields of all radiation emissions from the decaying radionuclide, the mass of the target region, and the absorbed fraction $\phi(r_T \leftarrow r_S, E_i)$*, the latter defined as the fraction of particle energy emitted within the source that is deposited in the target region:*

$$S(r_T \leftarrow r_S) = \frac{1}{m(r_T)} \sum_i E_i \, Y_i \, \phi(r_T \leftarrow r_S, E_i) = \sum_i \Delta_i \, \Phi(r_T \leftarrow r_S, E_i)$$

The S-value is a quantity unique to both a specific radionuclide (via the radionuclide decay scheme) and the geometric definitions of the source and target regions, along with any intervening tissues (via their spatial relationships, elemental compositions, and mass densities).

The MIRD schema is highly adaptable to a variety of dosimetric applications such that the source and target regions may encompass a range of anatomical scales from whole-organs, to sub-organ regions, to tissue layers, to cell clusters, to individual cells. The S-value may additionally be coupled with the 3D imaging data quantifying the radiopharmaceutical activities in the body tissues. This latter approach defines the S-value with respect to voxels in a reconstructed SPECT or PET image. Once the source and target regions are defined, Monte Carlo radiation transport is typically utilized to compute the absorbed fraction $\phi(r_T \leftarrow r_S, E_i)$*, although dose-point kernels may also be applied.*

3. Radionuclide S-Values – Organ Level

Radionuclide S-values at the organ level have traditionally been computed using computational phantoms of the human body that include all internal organs as potential source regions and all organs of radiogenic cancer risk as target regions.

Phantom Format Types

1. Stylized
2. Voxel
3. Hybrid/Mesh

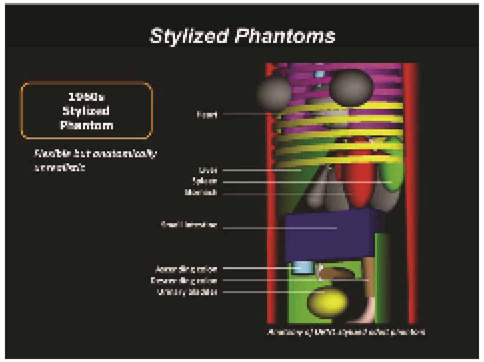

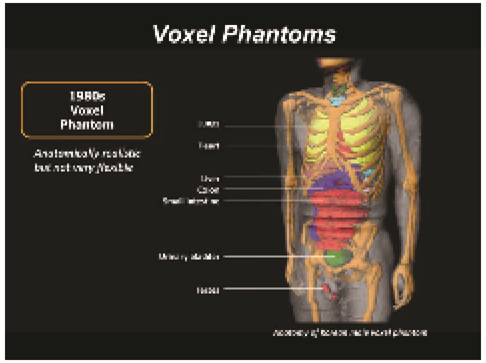

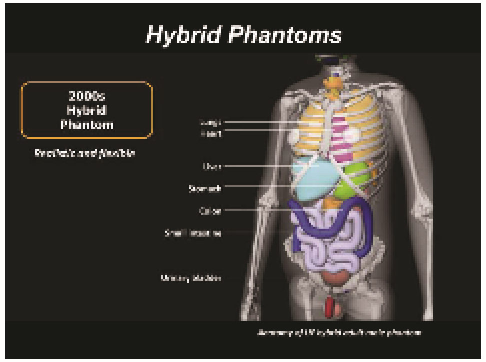

Phantom Morphometric Categories

1. Reference

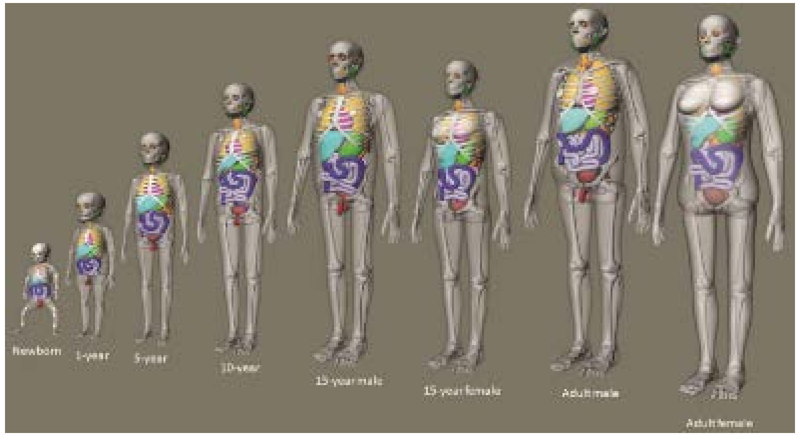

2. Patient-Dependent

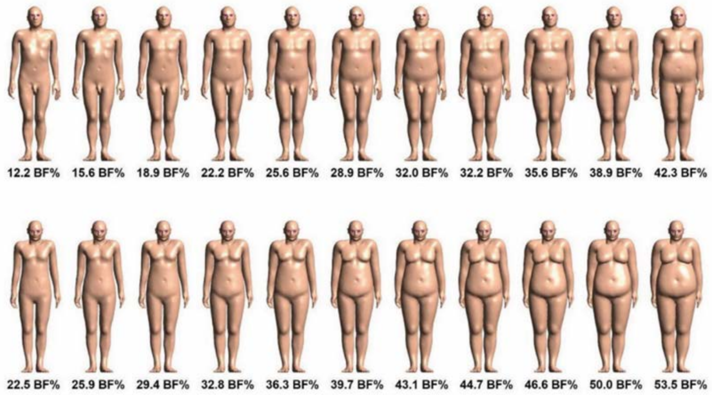

3. Patient-Sculpted
4. Patient-Specific

UF UNIVERSITY of FLORIDA
J. Crayton Pruitt Family Department of Biomedical Engineering

3. Radionuclide S-Values – Organ Level

Technical Note: Patient-morphed mesh-type phantoms to support personalized nuclear medicine dosimetry — a proof of concept study

Lukas M. Carter[a)] and Juan Camilo Ocampo Ramos
Department of Medical Physics, Memorial Sloan Kettering Cancer Center, New York, NY, USA

Wesley E. Bolch
J. Crayton Pruitt Family Department of Biomedical Engineering, University of Florida, Gainesville, FL, USA

Jason S. Lewis*
Department of Radiology, Program in Pharmacology and the Radiochemistry and Molecular Imaging Probes Core, Memorial Sloan Kettering Cancer Center, New York, NY, USA
Department of Radiology and Department of Pharmacology, Weill Cornell Medical College, New York, NY, USA

Adam L. Kesner*
Department of Medical Physics, Memorial Sloan Kettering Cancer Center, New York, NY, USA

Med. Phys. 48 (4), April 2021

Phantoms derived from PET/CT segmentation, and morphing of reference phantom via deformable image registration.

Volume-rendered CT (gray)
Exterior surfaces of segmented phantom (red)
Rigidly co-registered reference phantom (blue), and
Deformably co-registered reference phantom (green)

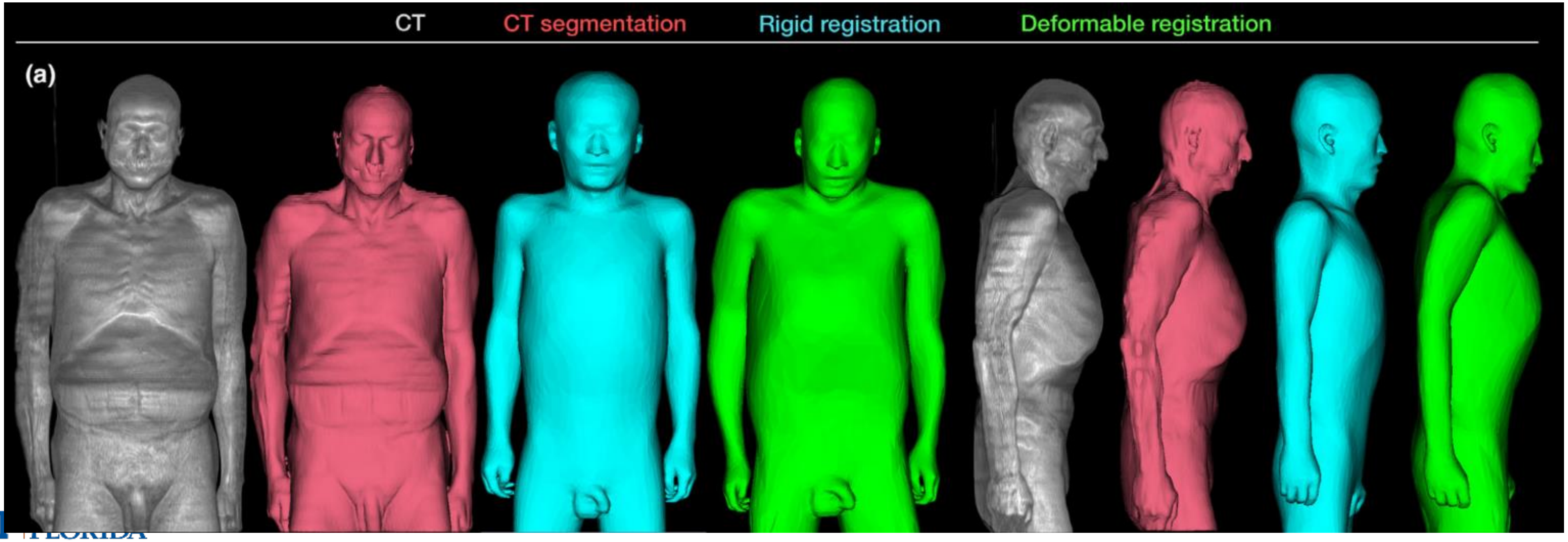

3. Radionuclide S-Values – Multiscale Dosimetry

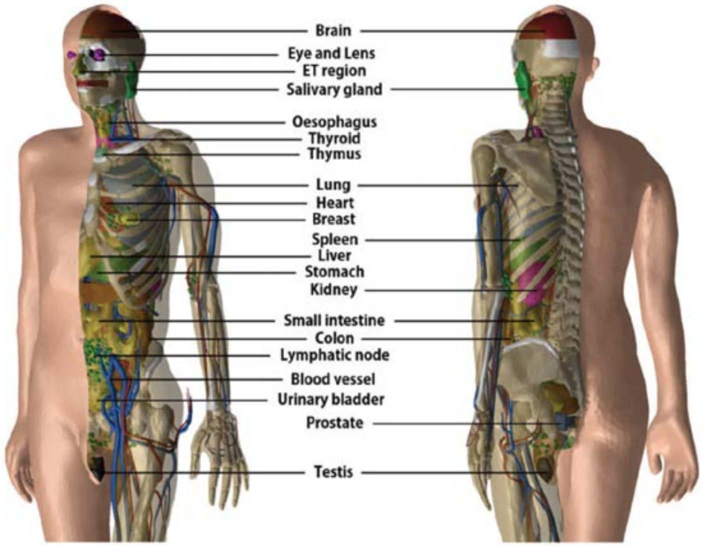

Whole Organs ⟵

Organ Subregions ⟶

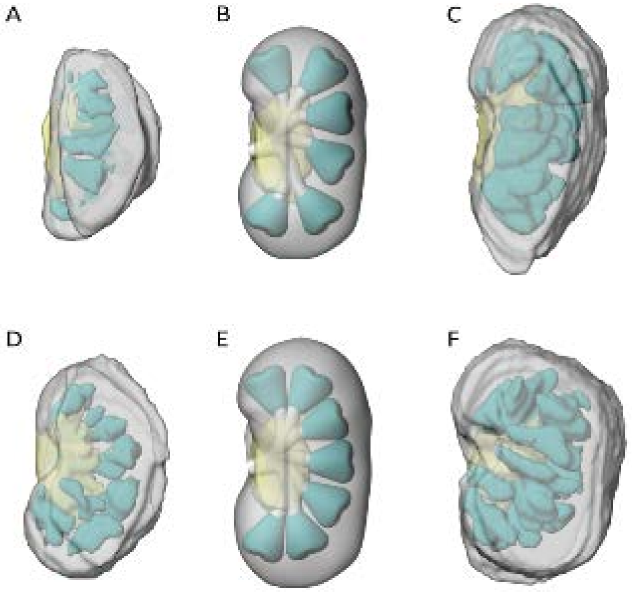

Regardless of the spatial scale, an implicit assumption in the MIRD schema is that the radiopharmaceutical is uniformly distributed across each individual source region r_S and dose is uniformly averaged across each individual target region r_T

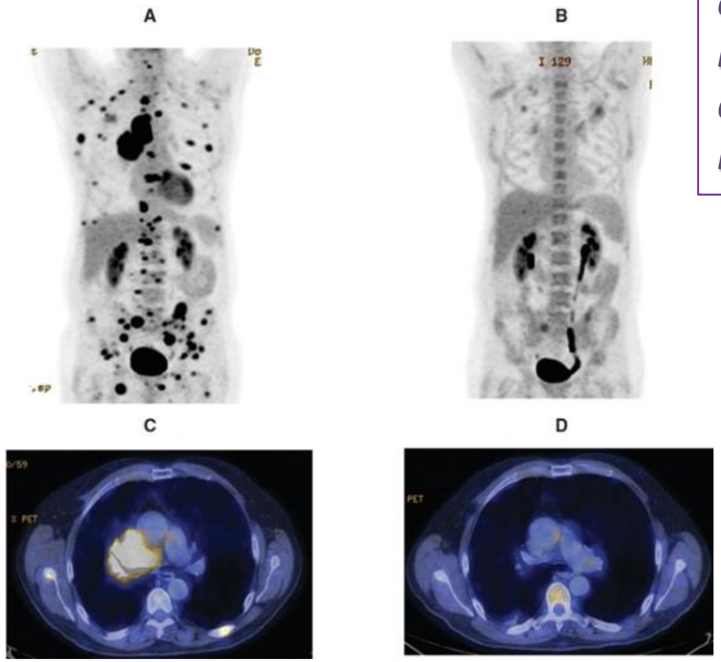

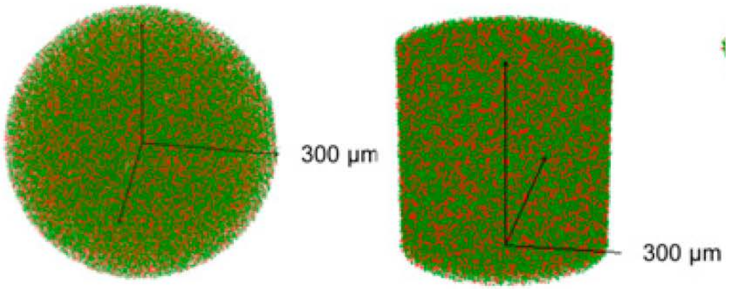

Image Voxels ⟵

Cells and Cell Clusters ⟶

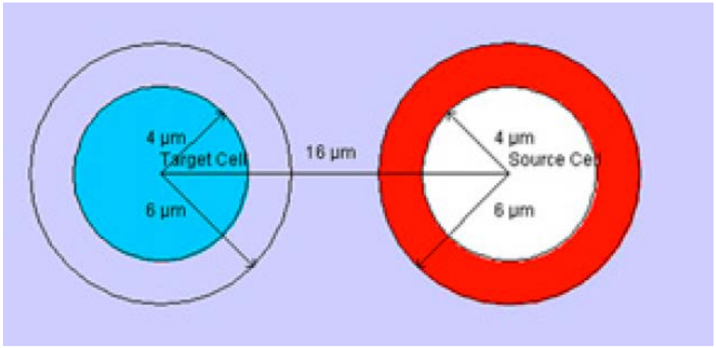

UF UNIVERSITY of FLORIDA
J. Crayton Pruitt Family Department of Biomedical Engineering

3. Radionuclide S-Values – Micro-to-Macro Approach

A nephron-based model of the kidneys for macro-to-micro α-particle dosimetry

Phys. Med. Biol. **57** (2012) 4403–4424

Robert F Hobbs[1,3], Hong Song[1], David L Huso[2], Margaret H Sundel[1] and George Sgouros[1]

[1] Department of Radiology, Johns Hopkins University, Baltimore MD, USA
[2] Department of Comparative Pathology, Johns Hopkins University, Baltimore MD, USA

$$D(TC) = \sum_{SC} g(SC)\,\tilde{A}(organ)\;S(TC \leftarrow SC)$$

SC – *source compartment (e.g., proximal tubules)*
TC **–** *target compartment (e.g., glomerulus)*

$\tilde{A}(organ)$ - *time-integrated activity imaged in the RPT patient*

$S(TC \leftarrow SC)$ – *microscale radionuclide S values for source/target compartments*
$g(SC)$ – *time integrated activity apportionment factor*

Microscale S values *– derived from either stylized models of organ microstructure, or developed through 3D tissue histology reconstructions.* ***TIA apportionment factors*** *must be developed through preclinical animal models to be extrapolated to the human patient.*

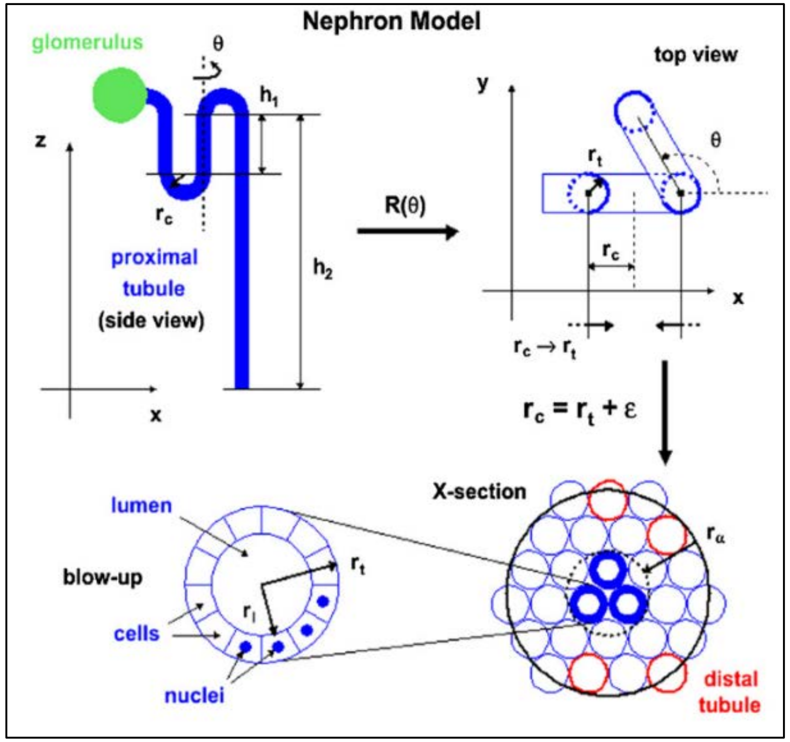

Table 2. Human microscale S values for the ^{225}Ac decay chain for both the unit and compartmental nephron model.

^{225}Ac	S-value (u) (Gy/Bq-s)	Absorbed energy (MeV/decay)	%	S-value (c) (Gy/Bq-s)
glc←glc	5.70E-05	5.24	88.07	1.85E-10
glc←prt	5.39E-06	0.75	12.61	6.08E-13
prtc←glc	3.02E-05	0.096	1.61	3.12E-12
prtc←prtc	4.54E-05	1.28	21.51	4.69E-12
prtc←prtl	4.49E-05	1.76	29.58	4.64E-12
prtc←prts	4.52E-05	1.53	25.71	4.66E-12
kid←kid	–	5.95	100.00	3.17E-12
cor←cor	–	5.95	100.00	4.82E-12

3. Radionuclide S-Values – Voxel Level

With the possible exception of tissue biopsy and blood sampling, 3D quantification of in-vivo radiopharmaceutical activity is limited to that seen in reconstructed SPECT and PET images of the RPT patient. With proper accounting for attenuation and scatter correction, as well as adjustments for partial volume effects, radiopharmaceutical activity may be quantified, to a given degree of uncertainty, at the image voxel level. These image voxels can thus serve as source regions, as well as target regions, under the MIRD schema provided that radionuclide S-values are available at the voxel level and at an equivalent scale and dimension.

- *Mathematical concept first proposed by Akabani et al. (1997) and Liu et al. (1998)*
- *MIRD Pamphlet No. 17 by Bolch et al. (1999)*
- *Franquiz et al. (2003) – expanded the availability of voxel S-values using DPKs to compute VSVs.*
- *Amato et al. (2012) – expanded their availability using GEANT4 radiation transport simulations.*
- *Lanconelli et al. (2012) published a web-accessible database for 7 radionuclides via EGSnrc.*

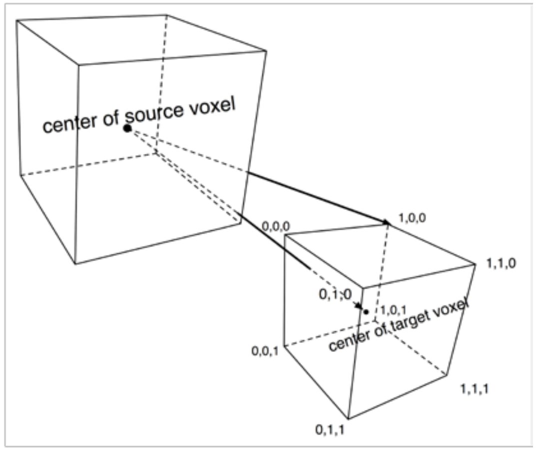

Applications:

- *^{153}Sm-EDTMP therapy for bone metastases (Feng et al. 2010)*
- *Comparison to organ-level dosimetry via OLINDA (Grimes and Celler 2014)*
- *DVH construction for ^{90}Y-DOTA-octreotide therapy (Li et al. 2018)*
- *Dose distributions following radionuclide-infused gold nanoparticles intra-tumoral injection therapy (Lai et al. 2017)*
- *Various studies comparing tissue dose distributions via VSV with those by PDK or direct MC (Mikell et al. 2015; Pacilio et al. 2015; Pacilio et al. 2009; Pasciak et al. 2014).*

Opportunities and Challenges

- *For radiation epidemiology studies for which some information exists on patient body morphometry, organ dosimetry should be based – not on methods taken from radiological protection using reference phantoms – but from explicit use of patient-dependent phantom libraries.*

- *For radiation epidemiology studies involving medical patients, the profession should implement strategies of organ dose assessment at the time of exposure. Examples might include:*
  - *Nuclear Medicine - MIRD calculations of organ doses from diagnostic and therapeutic imaging*
  - *Computed Tomography – Use CT image as the patient phantom or use phantom morphing techniques*
  - *Interventional fluoroscopy – Use RDSR files for post-surgery organ and skin dose reconstruction*
  - *External beam radiotherapy – both photon and proton – recording of in-field, near-field, and far-field organ doses*

- *For radiation epidemiology studies of internalized beta/alpha-emitting radionuclides:*
  - *Develop 3D models of tissue microstructure (Kidneys – model at the nephron level)*
  - *Use archived samples to determine 3D spatial distribution of deposition*
  - *At the whole-organ level, develop models of both intra-organ and inter-organ blood vasculature to differentiate between radionuclide decays in organ parenchyma from radionuclide decays in organ blood content*

Thank you for your attention. Would be happy to entertain any questions!

References – Monte Carlo Codes

Allison, J., Amako, K., Apostolakis, J., et al. (2016). 'Recent developments in Geant4'. *Nuclear Instruments and Methods in Physics Research Section A: Accelerators, Spectrometers, Detectors and Associated Equipment* **835**, 186-225.

Baró, J., Sempau, J., Fernández-Varea, J.M., and Salvat, F. (1995). 'PENELOPE: An algorithm for Monte Carlo simulation of the penetration and energy loss of electrons and positrons in matter'. *Nuclear Instruments and Methods in Physics Research Section B: Beam Interactions with Materials and Atoms* **100**, 31-46.

Berger, M.J. (1963). 'Monte Carlo calculation of the penetration and diffusion of fast charged particles', in: Alder, B., Fernbach, S., Rotenberg, M. (Eds.), Methods in Computational Physics. Academic Press, New York, pp. 163-215.

Berger, M.J. (1988). 'ETRAN — Experimental Benchmarks', in: Jenkins, T.M., Nelson, W.R., Rindi, A. (Eds.), Monte Carlo transport of electrons and photons. Plenum, New York, pp. 183-219.

Briesmiester, J.F. (1986). 'MCNP-A General Monte Carlo Code for Neutron and Photon Transport'. Los Alamos: Los Alamos National Laboratory.

Chiavassa, S., Bardies, M., Guiraud-Vitaux, F., et al. (2005). 'OEDIPE: a personalized dosimetric tool associating voxel-based models with MCNPX'. *Cancer Biother Radiopharm* **20**, 325-332. 10.1089/cbr.2005.20.325

Clairand, I., Ricard, M., Gouriou, J., Di Paola, M., and Aubert, B. (1999). 'DOSE3D: EGS4 Monte Carlo code-based software for internal radionuclide dosimetry'. *J Nucl Med* **40**, 1517-1523.

EGSnrc (2020). 'EGSnrc toolkit for Monte Carlo simulation of ionizing radiation transport'. https://github.com/nrc-cnrc/EGSnrc.

Ferrari, A., Sala, P.R., /CERN /INFN, M., et al. (2005). 'FLUKA: A Multi-Particle Transport Code'. ; Stanford Linear Accelerator Center (SLAC), p. Medium: ED; Size: 405 pages.

Friedland, W., Dingfelder, M., Kundrat, P., and Jacob, P. (2011). 'Track structures, DNA targets and radiation effects in the biophysical Monte Carlo simulation code PARTRAC'. *Mutat Res* **711**, 28-40.

Nikjoo, H., Emfietzoglou, D., Liamsuwan, T., et al. (2016). 'Radiation track, DNA damage and response-a review'. *Rep Prog Phys* **79**, 116601.

Perl J, Shin J, Schumann J, Faddegon B and Paganetti H 2012 TOPAS: an innovative proton Monte Carlo platform for research and clinical applications *Med Phys* **39** 6818-6837

Sarrut, D., Bardies, M., Boussion, N., et al. (2014). 'A review of the use and potential of the GATE Monte Carlo simulation code for radiation therapy and dosimetry applications'. *Med Phys* **41**, 064301.

Sato T, Iwamoto Y, Hashimoto S, Ogawa H, Furuta T, Abe S, Kai T, Tasi P, Matsuda N, Iwase H, Shigyo N, Sihver L and Nitta K 2018 Features of Particle and Heavy Ion Transport code system (PHITS) version 3.02 *J Nucl Sci Tech* **55** 684-690.

Seltzer, S.M. (1988). 'An overview of ETRAN Monte Carlo methods', in: Jenkins, T.M., Nelson, W.R., Rindi, A. (Eds.), Monte Carlo transport of electrons and and photons. Plenum, New York, pp. 153-182.

Semenenko, V.A., Turner, J.E., and Borak, T.B. (2003). 'NOREC, a Monte Carlo code for simulating electron tracks in liquid water'. *Radiat Environ Biophys* **42**, 213-217.

Song, H., Du, Y., Sgouros, G., et al. (2007). 'Therapeutic potential of ^{90}Y- and ^{131}I-labeled anti-CD20 monoclonal antibody in treating non-Hodgkin's lymphoma with pulmonary involvement: a Monte Carlo-based dosimetric analysis'. *J Nucl Med* **48**, 150-157.

Yoriyaz, H., Stabin, M.G., and dos Santos, A. (2001). 'Monte Carlo MCNP-4B-based absorbed dose distribution estimates for patient-specific dosimetry'. *J Nucl Med* **42**, 662-669.

References – Dose Point Kernels

Bardiès, M., and Myers, M.J. (1996). 'Computational methods in radionuclide dosimetry'. *Phys Med Biol* **41**, 1941-1955.

Cole, A. (1969). 'Absorption of 20-eV to 50,000-eV electron beams in air and plastic'. *Radiat Res* **38**, 7-33.

Cross, W.G. (1968). 'Variation of beta dose attenuation in different media'. *Phys Med Biol* **13**, 611-618.

Erdi, A.K., Yorke, E.D., Loew, M.H., et al. (1998). 'Use of the fast Hartley transform for three-dimensional dose calculation in radionuclide therapy'. *Med Phys* **25**, 2226-2233.

Gardin, I., Bouchet, L.G., Assie, K., et al. (2003). 'Voxeldose: A computer program for 3-D dose calculation in therapeutic nuclear medicine'. *Cancer Biother Radiopharm* **18**, 109-115.

Giap, H.B., Macey, D.J., Bayouth, J.E., and Boyer, A.L. (1995). 'Validation of a dose-point kernel convolution technique for internal dosimetry'. *Phys. Med. Biol.* **40**, 365-381.

Goddu, S.M., Howell, R.W., and Rao, D.V. (1994a). 'Cellular dosimetry: absorbed fractions for monoenergetic electron and alpha particle sources and S-values for radionuclides uniformly distributed in different cell compartments'. *J Nucl Med* **35**, 303-316.

Goddu, S.M., Rao, D.V., and Howell, R.W. (1994b). 'Multicellular dosimetry for micrometastases: dependence of self-dose versus cross-dose to cell nuclei on type and energy of radiation and subcellular distribution of radionuclides'. *J Nucl Med* **35**, 521-530.

Guy, M.J., Flux, G.D., Papavasileiou, P., Flower, M.A., and Ott, R.J. (2003). 'RMDP: a dedicated package for ^{131}I SPECT quantification, registration and patient-specific dosimetry'. *Cancer Biother Radiopharm* **18**, 61-69.

Howell, R.W., Rao, D.V., and Sastry, K.S. (1989). 'Macroscopic dosimetry for radioimmunotherapy: nonuniform activity distributions in solid tumors'. *Med Phys* **16**, 66-74.

Janicki, C., Duggan, D.M., Gonzalez, A., Coffey, C.W., 2nd, and Rahdert, D.A. (1999). 'Dose model for a beta-emitting stent in a realistic artery consisting of soft tissue and plaque'. *Med Phys* **26**, 2451-2460.

Kwok, C.S., Prestwich, W.V., and Wilson, B.C. (1985). 'Calculation of radiation doses for nonuniformly distributed beta and gamma radionuclides in soft tissue'. *Med Phys* **12**, 405-412.

Leichner, P.K. (1994). 'A unified approach to photon and beta particle dosimetry'. *J Nucl Med* **35**, 1721-1729.

Mangini, C.D., and Hamby, D.M. (2016). 'Scaling Parameters for Hot-Particle Beta Dosimetry'. *Radiat Prot Dosimetry* **172**, 356-366.

Sanchez-Garcia, M., Gardin, I., Lebtahi, R., and Dieudonne, A. (2014). 'A new approach for dose calculation in targeted radionuclide therapy (TRT) based on collapsed cone superposition: validation with ^{90}Y'. *Phys Med Biol* **59**, 4769-4784.

Sanchez-Garcia, M., Gardin, I., Lebtahi, R., and Dieudonne, A. (2015). 'Implementation and validation of collapsed cone superposition for radiopharmaceutical dosimetry of photon emitters'. *Phys Med Biol* **60**, 7861-7876.

Vaziri, B., Wu, H., Dhawan, A.P., Du, P., and Howell, R.W. (2014). 'MIRD Pamphlet No. 25: MIRDcell V2.0 Software Tool for Dosimetric Analysis of Biologic Response of Multicellular Populations'. *J Nucl Med* **55**, 1557-1564.

References – Voxel S Values

Akabani, G., Hawkins, W.G., Eckblade, M.B., and Leichner, P.K. (1997). 'Patient-specific dosimetry using quantitative SPECT imaging and three-dimensional discrete Fourier transform convolution'. *J. Nucl. Med.* **38**, 308-314.

Amato, E., Minutoli, F., Pacilio, M., Campenni, A., and Baldari, S. (2012). 'An analytical method for computing voxel S values for electrons and photons'. *Med Phys* **39**, 6808-6817.

Bolch, W.E., Bouchet, L.G., Robertson, J.S., et al. (1999). 'MIRD Pamphlet No. 17: The dosimetry of nonuniform activity distributions - Radionuclide S Values at the voxel level'. *J. Nucl. Med.* **40**, 11S-36S.

Feng, G., Lixin, C., Xiaowei, L., et al. (2010). 'A pilot study on the feasibility of real-time calculation of three-dimensional dose distribution for (153)Sm-EDTMP radionuclide therapy based on the voxel S-values'. *Cancer Biother Radiopharm* **25**, 345-352.

Franquiz, J.M., Chigurupati, S., and Kandagatla, K. (2003). 'Beta voxel S values for internal emitter dosimetry'. *Med Phys* **30**, 1030-1032.

Grimes, J., and Celler, A. (2014). 'Comparison of internal dose estimates obtained using organ-level, voxel S value, and Monte Carlo techniques'. *Med Phys* **41**, 092501.

Lai, P., Cai, Z., Pignol, J.P., et al. (2017). 'Monte Carlo simulation of radiation transport and dose deposition from locally released gold nanoparticles labeled with (111)In, (177)Lu or (90)Y incorporated into tissue implantable depots'. *Phys Med Biol* **62**, 8581-8599.

Lanconelli, N., Pacilio, M., Lo Meo, S., et al. (2012). 'A free database of radionuclide voxel S values for the dosimetry of nonuniform activity distributions'. *Phys Med Biol* **57**, 517-533.

Li, T., Wu, N.Y., Song, N., and Mok, G.S.P. (2018). 'Evaluation of sequential SPECT and CT for targeted radionuclide therapy dosimetry'. *Ann Nucl Med* **32**, 34-43.

Liu, A., Williams, L.E., Wong, J.Y., and Raubitschek, A.A. (1998). 'Monte Carlo-assisted voxel source kernel method (MAVSK) for internal beta dosimetry'. *Nucl Med Biol* **25**, 423-433.

Mikell, J.K., Mahvash, A., Siman, W., Mourtada, F., and Kappadath, S.C. (2015). 'Comparing voxel-based absorbed dosimetry methods in tumors, liver, lung, and at the liver-lung interface for ^{90}Y microsphere selective internal radiation therapy'. *EJNMMI Phys* **2**, 16.

Pacilio, M., Lanconelli, N., Lo Meo, S., et al. (2009). 'Differences among Monte Carlo codes in the calculations of voxel S values for radionuclide targeted therapy and analysis of their impact on absorbed dose evaluations'. *Med Phys* **36**, 1543-1552.

Pacilio, M., Amato, E., Lanconelli, N., et al. (2015). 'Differences in 3D dose distributions due to calculation method of voxel S-values and the influence of image blurring in SPECT'. *Phys Med Biol* **60**, 1945-1964.

Pasciak, A.S., Bourgeois, A.C., and Bradley, Y.C. (2014). 'A Comparison of Techniques for (90)Y PET/CT Image-Based Dosimetry Following Radioembolization with Resin Microspheres'. *Front Oncol* **4**, 121.